Comparing the ultraviolet photostability of azole chromophores

Chemical Science

Cite this: *Chem. Sci.*, 2012, **3**, 1192

www.rsc.org/chemicalscience

EDGE ARTICLE

Comparing the ultraviolet photostability of azole chromophores†

Gareth M. Roberts,[a] Craig A. Williams,[a] Martin J. Paterson,[b] Susanne Ullrich[c] and Vasilios G. Stavros*[a]

Received 1st December 2011, Accepted 4th January 2012
DOI: 10.1039/c2sc01000c

Ultrafast time-resolved velocity map imaging methods are used to interrogate the timescales for H-atom elimination in the azole isomers imidazole and pyrazole, the former of which is a prevalent moiety in biomolecules that exhibit a high degree of photostability following the absorption of ultraviolet (UV) radiation (*e.g.* DNA bases and aromatic amino acids). The results presented here, for the first time, draw focus on the statistical H-atom elimination dynamics in these two heteroaromatics, which result from vibrationally hot ground state (S_0) molecules that are formed following ultrafast internal conversion from an initially populated excited electronic state ($^1\pi\pi^*$ or $^1\pi\sigma^*$) at 200 nm. Measurements on imidazole suggest that statistical H-atom elimination is minimal over the temporal window of these experiments (which extends to 600 ps) and occurs on a timescale of >270 ps. Conversely, pyrazole shows a significant statistical H-atom yield by 600 ps with a time constant of 165 ± 30 ps. This highlights statistical unimolecular dissociation dynamics which, on these timescales, cannot be interpreted with traditional RRKM theory. Additional experiments on deuterated isotopomers of the two species also reveal that in imidazole statistical H-atom generation is localized to N–H bond fission, while in pyrazole there is approximately a 1 : 1 ratio between statistical C–H and N–H cleavage, and the two processes have associated time constants of 151 ± 20 ps and 193 ± 35 ps, respectively. We postulate that the observed high fraction of rapid irreversible C–H fission in pyrazole, relative to imidazole, may lead to the formation of toxic free radicals within specific biological environments, whereas statistical dissociation, restricted to only the N–H coordinate, may hypothetically quench UV photodamage yields *via* H-atom 'caging' and 'recombination' dynamics in hydrogen bonded networks (*e.g.* secondary protein structures).

1. Introduction

The relationship between molecular structure and function is critical throughout many areas of biology, and evolutionary selection has enabled biomolecules to become acutely tuned to perform these specific functions with exceptional levels of efficiency. Examples of this are prevalent in nature, highlighted by the cooperative O_2 binding mechanism in hemoglobin[1,2] and a wide variety of photolyase enzymes which target the repair of photodamaged DNA.[3,4] One of the cornerstone goals of modern biochemistry has been to intimately understand these highly specific processes in an effort to replicate and manipulate them. In the case of photo-initiated bio-cycles, the contemporary discipline of ultrafast biophysics has enabled a clearer insight into the origins of their efficiency.[5–9] Here, the role of the ensuing dynamics takes center stage, helping to elucidate how the molecular structure influences the overall function of the species, through a more comprehensive structure-*dynamics*-function approach. This technique has aided in intimately characterizing, amongst others, the trigger mechanism for human vision in rhodopsin,[10,11] charge-transfer processes in photosynthesis[12] and the origins of high fluorescence quantum yields in numerous fluorescent protein variants.[13–15]

In this work we apply this methodology as a potential stepping-stone towards understanding structural selectivity in biomolecules which display a high degree of photostability following absorption of ultraviolet (UV) radiation.[16–18] It has been postulated that, particularly on the pre-biotic earth, UV photostability played a critical role in the evolution of life[19] and today can act as a vital defense against harmful photo-induced genetic mutations.[18,20,21] The heteroaromatic UV chromophore imidazole (Fig. 1(a)) is found widely throughout this class of biomolecules: it is present within the purine derived DNA bases,[18] the amino acid histidine,[22] and importantly, also acts as a major UV absorber in the skin within urocanic acid.[23–25] This is in stark contrast to its structural isomer pyrazole (Fig. 1(b)), which is significantly more elusive in biological motifs,[26] particularly in photoprotection applications, yet its electronic

[a]*Department of Chemistry, University of Warwick, Library Road, Coventry, CV4 7AL, UK. E-mail: v.stavros@warwick.ac.uk*
[b]*Department of Chemistry, Heriot-Watt University, Edinburgh, EH14 4AS, UK*
[c]*Department of Physics and Astronomy, University of Georgia, Athens, Georgia, 30602, USA*
† Electronic supplementary information (ESI) available. See DOI: 10.1039/c2sc01000c

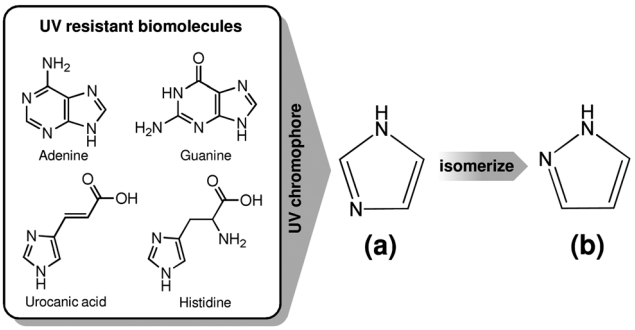

Fig. 1 Examples of biomolecules which are resistant to UV induced photodegradation and contain the heteroaromatic UV chromophore imidazole (a). Isomerization of imidazole yields the aromatic heterocycle pyrazole (b).

structure is qualitatively similar to that of imidazole.[27] Utilizing a combination of ultrafast time-resolved spectroscopy[28] and gas phase ion imaging techniques,[29] we seek to obtain a more complete picture of the UV induced dynamics occurring in these aromatic isomers. Specifically, we aim to illuminate any differences in their respective photochemistry.

Recent years have seen much interdisciplinary research devoted to untangling the origins of efficient UV photoprotection/photostability.[18,21] The seminal theoretical work of Sobolewski *et al.* provided one coherent explanation,[20] and implicated dissociative $^1\pi\sigma^*$ electronic excited states, localized along X–H bonds (X = N or O), as a means for rapidly and harmlessly dissipating excess UV photon energy on ultrafast (femtosecond (fs)) timescales. This pathway, schematically represented in Fig. 2, ultimately yields relaxation to the electronic ground state (S_0) *via* conical intersections (CIs), or X–H fission (see Fig. 2(a)) and recombination in H-bonded species (*e.g.* DNA base pairs).[30,31]

In addition to these ultrafast kinetics, many gas phase experimental results[18] also implicate that undesired, but kinetically slower, 'statistical' fragmentation may play a role in the UV induced dynamics.[32–34] In this process, the nascent energy in S_0, following internal conversion (IC) from the $^1\pi\sigma^*$ state at the $^1\pi\sigma^*/S_0$ CI, may induce molecular fragmentation, resulting in a 'statistical boil-off' of H-atoms with low amounts of kinetic energy (see schematic in Fig. 2(b)). Previous experiments have often interpreted the dynamics of forming these 'statistical' H-atoms within an Rice–Ramsperger–Kassel–Marcus (RRKM) theory framework,[35,36] despite the fact that internal (vibrational) energy following IC onto S_0 at the $^1\pi\sigma^*/S_0$ CI is not in an equilibrated state—as required in an RRKM treatment—rather, internal energy is likely to be localized along the X–H bond dissociation coordinate.

This statistical H-atom elimination behavior is traditionally considered a gas phase phenomenon. However, the gas phase often provides an excellent model for studying *in vivo* dynamics in proteins/hydrophobic cavities (such as the core of a DNA duplex or a protein chromophore pocket[37,38]), as the dielectric constant, ε, in these environments (ε = 3–10) is more comparable to vacuum (ε = 1) than water (ε = 80).[39] With this in mind, it is therefore still imperative that photostable chromophores efficiently partition excess vibrational energy into intramolecular 'bath' modes of the surrounding environment (*e.g.* an extended protein manifold) to not only avoid extensive fragmentation/

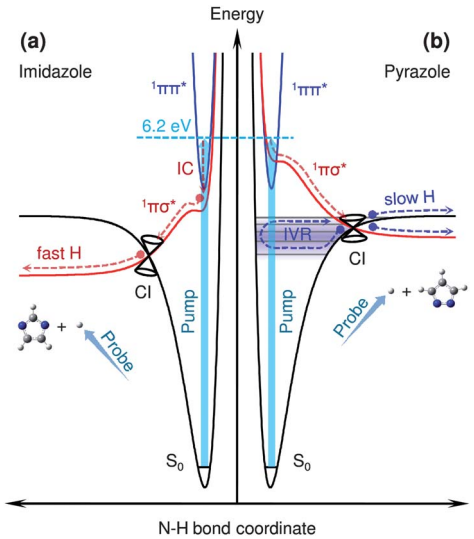

Fig. 2 Schematic potential energy cuts of the electronic ground (S_0) and excited ($^1\pi\pi^*$, $^1\pi\sigma^*$) states in (a) imidazole and (b) pyrazole, with respect to their N–H bond coordinates, R_{N-H}. These schematics are adapted from previously calculated potential energy profiles along R_{N-H} in ref. 27. Following excitation at 200 nm (6.2 eV) with a fs pump pulse, (a) presents a representative pathway for ultrafast relaxation and N–H bond fission *via* internal conversion (IC) at conical intersections (CIs), resulting in the formation of H-atoms with high amounts of kinetic energy (fast H) together with associated aromatic radical co-fragments. H-atoms are ionized and detected using a second temporally delayed fs probe pulse in our experimental detection scheme (inset). (b) shows how coupling back to S_0 *via* a $^1\pi\sigma^*/S_0$ CI results in vibrationally hot S_0 species, which may then undergo internal vibrational energy redistribution (IVR) and the loss of 'statistical' H-atoms that possess low amounts of kinetic energy (slow H).

photodegradation of the UV chromophore, but to also negate the production of toxic free radicals.[40] Additionally, during gas phase reactions that generated fundamental organic precursors for life on the pre-biotic earth,[19] which lacked any significant atmospheric (ozone) shielding from extraterrestrial UV radiation, degradative UV induced photochemistry, such as statistical fragmentation, may have influenced a structural bias towards photostable 'building-blocks' for simple self-replicating molecules and eventually life.

In this study we investigate statistical H-atom loss from both imidazole and pyrazole in the gas phase following UV excitation with a fs laser pulse, and monitor the yield of nascent H-atoms with a temporally delayed ionization laser pulse to generate H^+ using resonance enhanced multiphoton ionization (REMPI). H^+ is subsequently detected as a function of kinetic energy using velocity map ion imaging.[41] The combination of these two techniques has allowed us, for the first time, to extract the timescales for the 'statistical' H-atom elimination pathways in these two species, revealing that the timescales for this process occur over hundreds of ps, indicative of dynamics that are not governed by RRKM behavior.

2. Experimental methods

The setup utilized to probe the photochemistry of imidazole and pyrazole has been reported previously[42] and additional details

are provided in the electronic supplementary information (ESI†) online. Briefly, imidazole or pyrazole (Sigma-Aldrich, >98%) is seeded in helium (~2 bar) and introduced into a velocity map imaging (VMI)[29] spectrometer using an Even–Lavie pulsed valve which is heated to ~100 °C.[43] Dynamics are initiated using 200 nm fs laser pulses (pump), which are derived from the fundamental output (800 nm) of an amplified Ti:Sapphire laser system. Any nascent H-atoms subsequently undergo REMPI as a function of time (Δt), using temporally delayed 243.1 nm fs pulses (probe), two photons of which are resonant with the 2s ← 1s transition in H. H^+ is then detected as a function of both time and kinetic energy using time-resolved VMI. The desired total kinetic energy release (TKER) spectra are derived from the measured H^+ images using a polar onion-peeling algorithm,[44] together with an appropriate Jacobian and calibration factor,[45] assuming $C_3N_2H_3$ as the radical co-fragments of the dissociation process. For these experiments, the Gaussian laser cross-correlation was measured to be ~160 fs full width at half maximum (FWHM).

Experiments were also performed on deuterated isotopomers of both imidazole and pyrazole: imidazole-d_1, pyrazole-d_1 and pyrazole-d_3. These isotopomers were synthesized in-house from undeuterated samples of the two species (see ESI†). For these isotopomers, in addition to measurements utilizing time-resolved REMPI and VMI of eliminated H-atoms, results are also recorded for VMI of photodissociated and REMPI probed deuterium atoms (D^+) using the same experimental conditions described above.

3. Results

3.1 Identification and separation of statistical and $^1\pi\sigma^*$ H-atom elimination

Fig. 3 displays TKER spectra of REMPI probed H-atoms (H^+) which have been generated following 200 nm excitation of (a) imidazole and (b) pyrazole at $\Delta t = 2.5$ ps and 600 ps. The 200 nm pump wavelength has been selected as the strong absorption onset for both imidazole and pyrazole occurs at ~220 nm[46,47] (corresponding to the onset of the first $^1\pi\pi^*$ ← S_0 transition in both species, shown in Fig. 2). The corresponding H^+ velocity map images, from which the TKER spectra are derived, are shown in the inset of Fig. 3; counts at the center of the images correspond to low kinetic energy (KE) H^+ while signals at larger radii correlate to H^+ with higher KEs. We also highlight that there is negligible signal at negative Δt values and that detuning the probe away from its REMPI transition ($\lambda \neq 243.1$ nm) results in no H^+, indicative of only probing H-atoms in our pump–probe scheme.

The TKER spectra for both species recorded at 2.5 ps display Gaussian shaped features centered at ~10 000 cm^{-1}. These signals have previously been assigned to probed H-atoms generated *via* ultrafast N–H fission along $^1\pi\sigma^*$ states (depicted in Fig. 2(a)), and transients for these integrated features yield timescales of <80 fs for this pathway in both systems.[45,48] With reference to Fig. 2, in imidazole this signal results from initial population of the bright $^1\pi\pi^*$ state followed by IC to the $^1\pi\sigma^*$ surface (*via* an out-of-plane ring distortion coordinate[49]) and subsequent H-atom elimination,[48] while in pyrazole the $^1\pi\sigma^*$

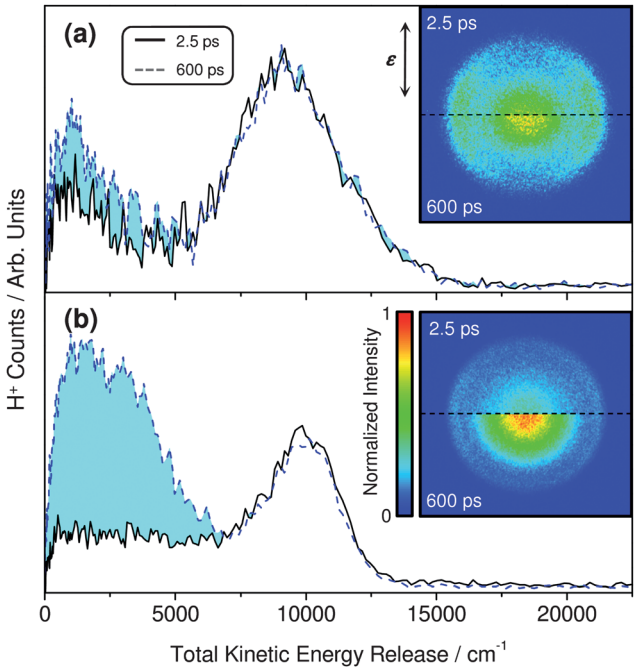

Fig. 3 Raw H^+ images and derived TKER spectra for (a) imidazole and (b) pyrazole, recorded at pump–probe delays (Δt) of 2.5 ps and 600 ps. The polarization of the pump laser, ε, is shown inset. Blue shading highlights the increase in H^+ counts at low kinetic energies, corresponding to an enhancement of probed 'statistical' H-atoms between 2.5 ps and 600 ps.

manifold is directly populated at 200 nm (in addition to the $^1\pi\pi^*$ state) causing extremely rapid (<50 fs) N–H bond rupture.[45] We do not consider these high KE signals in any greater detail here, only to state that upon extending these transients out to 600 ps (provided in the ESI†), no additional H^+ signal increase is observed, indicating that direct N–H fission dynamics *via* the $^1\pi\sigma^*$ surface are over by ~300 fs. This is also evidenced by the TKER spectra and H^+ velocity map images provided in Fig. 3 at 2.5 ps *vs.* 600 ps.

We now focus on the H^+ signal localized at low KEs (<5000 cm^{-1}) with 'Boltzmann-like' profiles. At 2.5 ps we have previously attributed these REMPI probed H-atoms to be multi-photon *and* multicomponent in nature (*e.g.* dissociative ionization of hot parent cations),[45,48] as their corresponding appearance times are both less than 200 fs, far too rapid for a statistical decay process (*typically* $\geq 10^{-10}$ s).[50] The low KE features of the TKER spectra for $\Delta t \leq 2.5$ ps have previously been discussed in depth in ref. 45 and 48, and their pertaining dynamics do not affect the ensuing arguments. As such, we do not discuss these in any further detail here. When we extend these measurements out to longer time delays (600 ps) in imidazole (Fig. 3(a)) we see that there is a minor increase in the H^+ yield at low KEs (blue shading). Conversely, for pyrazole (Fig. 3(b)) there is a pronounced gain in H^+ counts below 5000 cm^{-1} by 600 ps. We postulate that this additional increase in low KE H^+ signal correlates to REMPI of H-atoms which are generated through statistical decay processes from a highly vibrationally excited S_0 state in the neutral parent species; a possible pathway for this statistical mechanism is represented in Fig. 2(b). Alternatively, these probed statistical H-atoms may hypothetically

occur from dissociation of vibrationally hot photofragments, which are all initially formed in <200 fs after UV excitation,[45] although they constitute a very minor fraction of the overall photochemistry at 200 nm (~10% in imidazole).[51] However, based on considerations of the thermochemistry of both imidazole and pyrazole[52,53] (and related heteroaromatics[54]), we conclude that successive fragmentations to generate H-atoms is thermodynamically unfeasible following excitation at 200 nm. Importantly, we emphasize that relative to pyrazole, the statistical H-atom signal observed in imidazole by 600 ps is comparatively small, providing a preliminary indication that the yield for statistical H-atom generation in imidazole is notably less than that of its structural isomer pyrazole.

3.2 Timescales for statistical H-atom elimination

To investigate the timescales for these statistical H-atom elimination processes in a more quantitative manner, Fig. 4 presents the normalized H^+ transients for the low KE features in Fig. 3 up to 600 ps. These have been obtained by integrating the low KE signals over a defined energy window (200–1000 cm^{-1}) at each Δt. The sharp rise in both transients at $\Delta t = 0$ ps is due to contributions from a variety of ultrafast multiphoton processes, as discussed briefly above and in detail in refs. 45 and 48. In imidazole a steady but minimal increase in signal is observed by 600 ps, at which time the dynamics appear to still be ongoing (*i.e.* the H^+ yield appears not to have plateaued), whereas pyrazole presents a larger and more rapid rise in signal that begins to level off around 400 ps. Fits to these transients using exponential rise functions convoluted with the Gaussian instrument response function (FWHM ~ 160 fs), shown as solid lines in Fig. 4 (see ESI† for fit details), provide statistical H-atom elimination timescales for imidazole and pyrazole of >270 ps and 165 ± 30 ps, respectively, as summarized in Table 1. Due to the continuing rise in H^+ signal by 600 ps in the experimental transient for imidazole, we quote the extracted time constant as a lower limit.

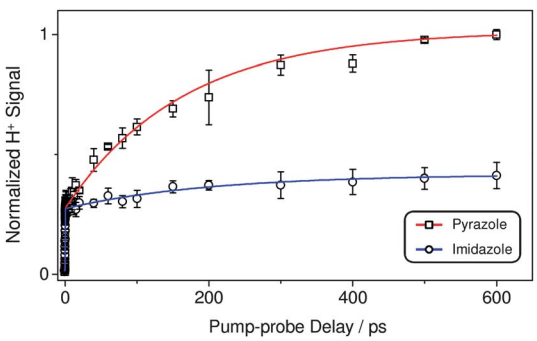

Fig. 4 Integrated H^+ signal transients (200–1000 cm^{-1}) for the low kinetic energy components in the TKER spectra of imidazole and pyrazole (circles and squares, respectively). Error bars correspond to two standard deviations of the mean signal values (two σ). Fits to the two transients using exponential functions convoluted with the Gaussian instrument response function are shown by the solid lines (see ESI† for fit details). Time constants extracted from these fits are provided in Table 1. The two transients have been normalized based on the sharp signal steps at a pump–probe delay of $\Delta t = 0$ ps, to emphasize the differences in H^+ signal increase between the two species at longer pump–probe delays.

At this stage we emphasize a number of key points. (i) The imidazole time constant provides a *very conservative* lower limit to statistical H-atom elimination, as the experimental transient in Fig. 4 suggests that the time constant for this process may be >600 ps, due to dynamics which are still ongoing by the temporal limits of our experiment (Δt = 600 ps). (ii) The measurements presented in Fig. 4 do not elucidate the exact origins of the observed statistical H-atoms, as there may be mixed contributions from both N–H and C–H fissions following internal vibrational energy redistribution (IVR) on S_0. Finally, (iii) the mechanism for repopulating S_0 may be *via* coupling at the $^1\pi\sigma^*/S_0$ CI, yet we cannot rule out other relaxation channels from the optical bright $^1\pi\pi^*$ state through $^1\pi\pi^*/S_0$ CIs located along other nuclear degrees of freedom, as predicted by *ab initio* calculations in imidazole.[49] For pyrazole, we have performed *ab initio* calculations which reveal that a $^1\pi\pi^*/S_0$ CI does indeed exist, suggesting that it is in principle possible for population in pyrazole's $^1\pi\pi^*$ state to directly couple into a vibrationally hot S_0; further details are provided in the ESI†. In the succeeding section we endeavor to address the issue of untangling potential mixed contributions from statistical C–H and N–H cleavage through further experiments which utilize deuterated isotopomers of imidazole and pyrazole.

3.3 Elucidation of statistical decay pathways along C–H and N–H coordinates

To gain some insight into contributions from C–H fission, d_1 isotopomers (N-D substitution) were used to block contributions from N–H fission, while the d_3 species (C-D substitution) terminates H-atom elimination from all C–H coordinates.

In imidazole-d_1, negligible H^+ signal is observed following photolysis at 200 nm, indicating that the small increase in statistical decay counts measured in the undeuterated imidazole transient (Fig. 4) is indeed localized to N–H dissociation. As a result of this, and due to complexities in synthesizing imidazole-d_3, additional measurements for imidazole's d_3 isotopomer are not discussed here.

H^+ imaging measurements on pyrazole-d_1 and pyrazole-d_3 have also been performed, the results of which are presented in Fig. 5 (molecular structures inset). The TKER spectrum of pyrazole-d_1, shown in Fig. 5(a) for Δt = 2.5 ps and 600 ps, reveals that there is still some fraction of H^+ signal increase at low KEs. Notably, the Gaussian feature observed at higher KEs in undeuterated pyrazole (Fig. 3(b)) is almost completely eliminated, as expected due to termination of direct $^1\pi\sigma^*$ mediated H-atom elimination—the small Gaussian profile observed around ~10 000 cm^{-1} in Fig. 5(a) is due to a minor contamination of N–H fission from undeuterated pyrazole (see ESI†). The increase in H^+ counts at low KEs in Fig. 5(a) very likely results from REMPI probed H-atoms following statistical C–H scission, suggesting that a notable element of the low KE signal increase observed in pyrazole (Fig. 3(b) and Fig. 4) arises due to this fragmentation process. Kinetic fits to a transient of this feature, shown in Fig. 5(b), extract a timescale of τ_{CH} = 151 ± 20 ps for statistical C–H cleavage. Similarly, the pyrazole-d_3 TKER spectra at Δt = 2.5 ps and 600 ps are also provided in Fig. 5(c). Here, a distinct signal increase is still observed at low KEs, which we logically assign to statistical H-atom loss from the N–H coordinate.

Table 1 Statistical H-atom elimination time constants, τ_{obs}, for imidazole and pyrazole, together with time constants for statistical N–H, τ_{NH}, and C–H fission, τ_{CH}, obtained from pyrazole-d_3 and pyrazole-d_1 isotopomers, respectively. Also presented are the relative branching fractions for statistical C–H and N–H fission in the two species, A_{NH} and A_{CH}, respectively, obtained from analyzing TKER spectra derived from H^+ and D^+ velocity map images of pyrazole-d_1 and pyrazole-d_3 (see text for details). Averages of the two A_{NH} and A_{CH} values are also provided

				Pyrazole-d_1		Pyrazole-d_3		Average	
Molecule	τ_{obs}/ps	τ_{NH}/ps	τ_{CH}/ps	A_{NH}	A_{CH}	A_{NH}	A_{CH}	A_{NH}	A_{CH}
Imidazole	>270	—	—	—	—	—	—	1	0
Pyrazole	165 ± 30	193 ± 35	151 ± 20	0.37	0.63	0.54	0.46	0.45	0.55

Integration of this feature at each Δt in pyrazole-d_3 yields the transient in Fig. 5(d), which when fitted provides a time constant of $\tau_{NH} = 193 \pm 35$ ps.

By comparing TKER spectra derived from both H^+ and D^+ velocity map images of pyrazole-d_1 (Fig. 6(a)) and pyrazole-d_3 (Fig. 6(b)), some insight into the relative contributions for C–H and N–H fission to the low KE signal in undeuterated pyrazole can be obtained. For pyrazole-d_1 these TKER spectra are provided in Fig. 6(a), where the H^+ and D^+ derived spectra are shown by the dashed red and blue lines and result from C–H and N–D fission, respectively. The sum of the two spectra is also provided (black line), and is in good accord with the profile of the H^+ derived TKER spectrum recorded for undeuterated pyrazole (gray line). Evaluation of the $H^+ : D^+$ signal ratio at low KEs implicates that the fraction of signal associated with N–H fission in the undeuterated species, A_{NH}, is 0.37, together with a value of 0.63 for the quotient of H-atoms generated through C–H cleavage, A_{CH}. These values are summarized in Table 1 and a detailed method of their derivation is provided in the ESI†.

An analogous analysis of the spectra obtained for pyrazole-d_3, yields $A_{NH} = 0.54$ and $A_{CH} = 0.46$, which vary from the values extracted from pyrazole-d_1 measurements. With this in mind, we note that this analysis does not consider differences arising from isotopic substitution, such as modified bond strengths and differences in elimination timescales for H and D atoms, which may manifest as variations in A_{NH} and A_{CH} between the two isotopomers. However, in both cases the sum of the H^+ and D^+ derived TKER spectra compare very well with the profile of the TKER spectrum measured for undeuterated pyrazole, suggesting that there is some validity to this approach. Taking this into consideration, we elect to calculate an average of the A_{NH} and A_{CH} values obtained from both isotopomers, implying that ~50% of probed statistical H-atoms arise from C–H scission (see Table 1). Despite the simplistic nature of this interpretation, further justification for this approach is garnered by using these average A_{NH} and A_{CH} values to determine a weighted time constant of ~170 ps ($\tau_{obs} = A_{NH}\tau_{NH} + A_{CH}\tau_{CH}$), which is commensurate with $\tau_{obs} = 165 \pm 30$ ps extracted from undeuterated pyrazole.

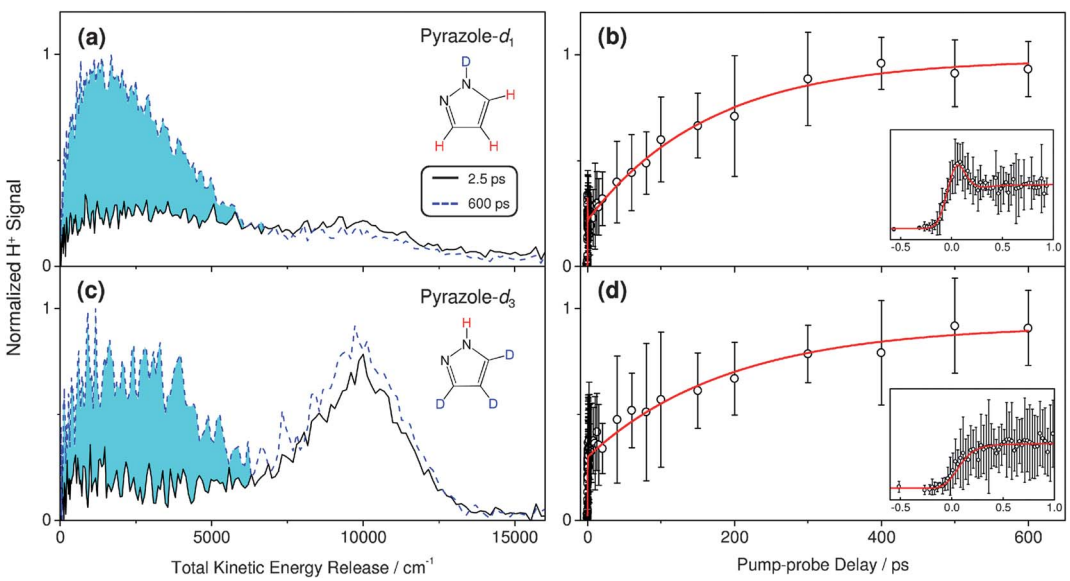

Fig. 5 (a) TKER spectra derived from the H^+ velocity map images for pyrazole-d_1 (structure inset), recorded at $\Delta t = 2.5$ ps and 600 ps, together with (b) the associated low kinetic energy H^+ signal transient (circles) and temporal fit (red line). The H^+ derived TKER spectra for pyrazole-d_3 (structure inset in (c)), at $\Delta t = 2.5$ ps and 600 ps, and associated low kinetic energy H^+ signal transient with fit are also shown in (c) and (d), respectively. Error bars on signal transients correlate to two standard deviations of the mean signal (two σ). Insets in (b) and (d) show the low kinetic energy H^+ signal transients at early pump–probe delays, up to $\Delta t = 1$ ps. Blue shading in the TKER spectra highlights the increase in H^+ counts at low kinetic energies.

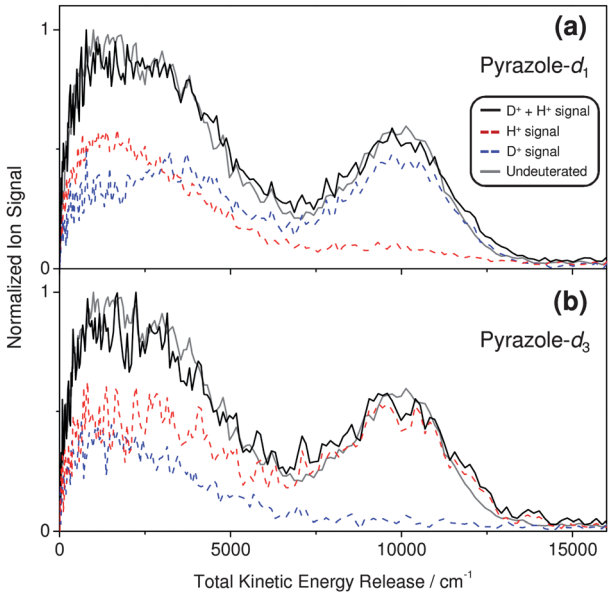

Fig. 6 (a) TKER spectra derived from recorded H^+ and D^+ velocity map images from pyrazole-d_1 at Δt = 600 ps (red and blue dashed lines, respectively). These spectra have been normalized with respect to the sum of these two spectra, shown by the black line. Also presented is the normalized TKER spectrum for undeuterated pyrazole (grey line) at Δt = 600 ps. (b) Analogous TKER spectra recorded for pyrazole-d_3.

4. Discussion

4.1 Comparison with RRKM theory

Previous studies have interpreted the low KE 'Boltzmann-like' H^+ signals in terms of statistical unimolecular dissociation kinetics within RRKM theory, which assumes that internal (vibrational) energy is *fully equilibrated* in the system.[50] Focusing, to begin with, on statistical H-loss from the N–H coordinate in imidazole, for a vibrationally hot S_0 state with 50 000 cm^{-1} of internal energy, RRKM calculations predict a unimolecular dissociation time constant of ~20 ns (see ESI† for calculation details). A similar calculation in pyrazole provides a theoretical timescale of ~700 ns for statistical N–H fission, both of which are significantly longer than the hundreds of ps timescales we observe here for 'statistical' H-atom elimination from a hot S_0 manifold. At first glance this may suggest these H-atoms are generated *via* a different mechanism, the most feasible of which would appear to be some 'frustrated' dissociation event, as previously proposed in pyrrole.[55] In imidazole and pyrazole, such a process would require that the $^1\pi\sigma^*$ surfaces are not purely repulsive with respect to the N–H coordinate, enabling some population to be trapped in a bound region (*cf.* the lowest energy $^1\pi\sigma^*$ state in aniline[56]), which may then 'leak' out on a timescale slower than the direct $^1\pi\sigma^*$ mediated N–H fission discussed in section 3.1. Consultation of the calculated potential energy profiles of the $^1\pi\sigma^*$ states suggests that no bound regions exist,[27] making frustrated dissociation a tenuous interpretation and adding further weight to our postulate that statistical H-atoms are generated from vibrationally hot S_0 species.

The fact that the statistical H-atom elimination dynamics we observe here occur over the order of hundreds of ps is indicative of unimolecular dissociation which cannot be interpreted with respect to an RRKM model; hence, the lack of agreement between our experimentally determined rates and RRKM predicted rates. This is in some ways profoundly logical, as following repopulation of the S_0 *via* vibrational coupling at CIs, vibrational flux will be distinctly localized in specific nuclear degrees of freedom (which may then over time undergo IVR). This scenario stands entirely at odds with one of the central assumptions of RRKM theory, that the internal energy of the system in question is *fully equilibrated*. As such our results clearly emphasize that the *dynamics* for forming statistical H-atoms, which contribute to these low KE signals, cannot be modelled within a simple RRKM framework (as has been done in past studies,[35,36] although we note that some previous measurements were recorded at time delays of 10s of ns where RRKM theory is more valid[35]). Furthermore, it may be plausible for analogous H-atom elimination pathways to manifest on similar timeframes (tens to hundreds of ps) in a variety of other heteroaromatic species (*e.g.* indoles and phenols).

4.2 Consideration of relative photostabilities

For the remainder of this discussion we consider the potential implications that statistical fragmentation kinetics may have on the apparent structural bias between these two heteroaromatic moieties in photoprotective/photostable biomolecules.

As an example, we consider this behavior in the context of UV chromophores embedded within large hydrophobic biological environments, such as proteins (ε = 3–10), which compare well with the gas phase (ε = 1). For imidazole, when localized within a hydrophobic cavity of an extended biomolecule (*e.g.* protein chromophore pockets[38] or DNA helices[37]), IVR into the global bio-structure may be in kinetic competition with the statistical H-loss kinetics we have observed to occur over hundreds of ps here. Notably, however, the yield for this H-loss channel by 600 ps appears to be relatively minor in imidazole. Converse observations in pyrazole of a comparatively high yield of rapid statistical H-atom elimination, within a temporal window of hundreds of ps, suggests that this pathway is more dominant, which could hypothetically be an undesirable characteristic for photostability in these biomolecules. We have also shown that statistical H-atom elimination dynamics in imidazole are highly localized to the N–H coordinate. In this scenario, the eliminated H-atoms may be recaptured within H-bonded motifs (*cf.* the amino acid histidine within a secondary protein structure). In pyrazole, this is not so as ~50% of the statistical H-atom loss results from fission of the C–H bonds, potentially leading to *irreversible* UV photodamage of the chromophore and the formation of highly reactive/toxic radicals.[40]

However, the studies presented in this Edge Article interrogate imidazole and pyrazole as isolated chromophores. In future studies it is therefore of particular interest to incrementally model the influences of larger biological structures to which they will be bonded. This may be achieved by increasing the molecular degrees of freedom in these systems (either *via* the addition of alkyl side-chains or with amino acids and polypeptides) and delivering these species into the gas phase with appropriate techniques, such as laser-desorption[57,58] and electrospray ionization[39,59,60] (particularly for charged species). We envisage (as

some precursor studies have demonstrated[34,61]) that as the density of internal states increases with added molecular complexity, statistical decay dynamics may begin to dominate the photochemistry in larger biological systems,[61] the timescales for which could become modified altogether.

We also recognize that the interpretation provided thus far considers hydrophobic environments in biology, within which imidazole moieties can often be found, for example histidine residues in proteins. Photobiology also takes place in free solvent.[38] In the condensed phase rapid intermolecular energy redistribution to the solvent will play a notable role.[21,62] Albeit this, the results here aim to provide a stepping-stone towards a more global understanding of UV photostability in aromatic heterocycles and mediate interest in exploring a wider theme of structural selectivity in photoresistant bio-chromophores.

5. Conclusions

Using time-resolved VMI experiments the timescales for statistical H-atom elimination channels, following irradiation at 200 nm, in imidazole and pyrazole have been quantified. Specifically, statistical H-atom loss from a vibrationally hot S_0 state in imidazole, which is formed following IC from an initially populated electronic excited state ($^1\pi\pi^*$ or $^1\pi\sigma^*$), occurs on a timescale >270 ps, with minimal probed statistical H-atom yield by 600 ps. In pyrazole, this H-loss mechanism appears to be more significant and takes place in 165 ± 30 ps. This study is the first to experimentally extract timescales for statistical H-atom elimination in these aromatic isomers. Comparative studies on deuterated isotopomers of the two azoles illuminate that in imidazole H-loss results from cleavage of the N–H bond only. In pyrazole there are approximately equal contributions from statistical C–H and N–H bond fissions, which possess time constants of 151 ± 20 ps and 193 ± 35 ps, respectively.

The statistical H-loss dynamics observed in these two species have been considered with respect to their effective photostabilities in biomolecules. Within the reasoning discussed here, the observed differences in photochemistry may have some bearing upon their effective photostability in hydrophobic environments in biology, such as proteins, together with possible implications for gaseous reactions on the pre-biotic earth. The results potentially offer some window of insight into untangling the origins of this structural bias, although it is critical to recognize that structural evolution/selection in nature is likely governed by many molecular characteristics, as opposed to photochemistry alone.

Acknowledgements

The authors gratefully thank Mr Dave Hadden for experimental assistance, Ms L. Therese Bergendahl for assistance with theory calculations, Dr David Fox and Prof. Richard Walton for help with preparing the deuterated isotopomers, Prof. Mike Ashfold for useful discussions, and Dr Jan Verlet for use of his polar onion peeling program. G.M.R thanks the Leverhulme Trust for postdoctoral funding. C.A.W thanks the EPSRC for a doctoral research fellowship. M.J.P thanks the European Research Council for funding under the European Union's Seventh Framework Programme (FP7/2007–2013)/ERC Grant No. 258990. S.U and V.G.S would like to thank the NSF and EPSRC for grants (NSF-CHE-0924456 and EP/H003401) which have been awarded through the International Collaboration in Chemistry Program. V.G.S would also like to thank the Royal Society for a University Research Fellowship and the University of Warwick for an RDF award.

References

1 A. V. Hill, *J. Physiol.*, 1910, **40**, iv–vii.
2 S. J. Edelstein, *Annu. Rev. Biochem.*, 1975, **44**, 209–232.
3 A. Sancar, *Chem. Rev.*, 2003, **103**, 2203–2237.
4 J. Li, Z. Y. Liu, C. Tan, X. M. Guo, L. J. Wang, A. Sancar and D. P. Zhong, *Nature*, 2010, **466**, 887–890.
5 A. Holzwarth, *Q. Rev. Biophys.*, 1989, **22**, 239–326.
6 J. L. Martin and M. H. Vos, *Annu. Rev. Biophys. Biomol. Struct.*, 1992, **21**, 199–222.
7 M. T. Zanni and R. M. Hochstrasser, *Curr. Opin. Struct. Biol.*, 2001, **11**, 516–522.
8 N. T. Hunt, *Chem. Soc. Rev.*, 2009, **38**, 1837–1848.
9 A. H. Zewail and M. Chergui, *ChemPhysChem*, 2009, **10**, 28–43.
10 P. Kukura, D. W. McCamant, S. Yoon, D. B. Wandschneider and R. A. Mathies, *Science*, 2005, **310**, 1006–1009.
11 M. Garavelli, D. Polli, P. Altoe, O. Weingart, K. M. Spillane, C. Manzoni, D. Brida, G. Tomasello, G. Orlandi, P. Kukura, R. A. Mathies and G. Cerullo, *Nature*, 2010, **467**, 440–443.
12 H. Y. Wang, S. Lin, J. P. Allen, J. C. Williams, S. Blankert, C. Laser and N. W. Woodbury, *Science*, 2007, **316**, 747–750.
13 P. J. Tonge, M. Kondo, I. A. Heisler, D. Stoner-Ma and S. R. Meech, *J. Am. Chem. Soc.*, 2010, **132**, 1452–1453.
14 K. M. Solntsev, J. Conyard, M. Kondo, I. A. Heisler, G. Jones, A. Baldridge, L. M. Tolbert and S. R. Meech, *J. Phys. Chem. B*, 2011, **115**, 1571–1576.
15 I. R. Lee, W. Lee and A. H. Zewail, *Proc. Natl. Acad. Sci. U. S. A.*, 2006, **103**, 258–262.
16 P. Meredith and J. Riesz, *Photochem. Photobiol.*, 2004, **79**, 211–216.
17 P. R. Callis, in *Methods in Enzymology*, Academic Press, New York, 1997, vol. 278, p. 113.
18 C. E. Crespo-Hernandez, B. Cohen, P. M. Hare and B. Kohler, *Chem. Rev.*, 2004, **104**, 1977–2019.
19 N. Balucani, *Int. J. Mol. Sci.*, 2009, **10**, 2304–2335.
20 A. L. Sobolewski, W. Domcke, C. Dedonder-Lardeux and C. Jouvet, *Phys. Chem. Chem. Phys.*, 2002, **4**, 1093–1100.
21 C. T. Middleton, K. de La Harpe, C. Su, Y. K. Law, C. E. Crespo-Hernandez and B. Kohler, *Annu. Rev. Phys. Chem.*, 2009, **60**, 217–239.
22 H. Du, R. C. A. Fuh, J. Z. Li, L. A. Corkan and J. S. Lindsey, *Photochem. Photobiol.*, 1998, **68**, 141–142.
23 M. Norval, *Prog. Biophys. Mol. Biol.*, 2006, **92**, 108–118.
24 K. M. Hanson and J. D. Simon, *Proc. Natl. Acad. Sci. U. S. A.*, 1998, **95**, 10576–10578.
25 E. C. De Fabo and F. P. Noonan, *J. Exp. Med.*, 1983, **158**, 84–98.
26 T. Eicher and S. Hauptmann, *The Chemistry of Heterocycles: Structure, Reactions, Syntheses, and Applications*, Wiley-VCH, Berlin, Germany, 2003.
27 G. A. King, T. A. A. Oliver, M. G. D. Nix and M. N. R. Ashfold, *J. Chem. Phys.*, 2010, **132**, 064305.
28 A. H. Zewail, *J. Phys. Chem. A*, 2000, **104**, 5660–5694.
29 A. T. J. B. Eppink and D. H. Parker, *Rev. Sci. Instrum.*, 1997, **68**, 3477–3484.
30 T. Schultz, E. Samoylova, W. Radloff, I. V. Hertel, A. L. Sobolewski and W. Domcke, *Science*, 2004, **306**, 1765–1768.
31 I. Hunig, C. Plutzer, K. A. Seefeld, D. Lowenich, M. Nispel and K. Kleinermanns, *ChemPhysChem*, 2004, **5**, 1427–1431.
32 M. N. R. Ashfold, B. Cronin, A. L. Devine, R. N. Dixon and M. G. D. Nix, *Science*, 2006, **312**, 1637–1640.
33 M. N. R. Ashfold, G. A. King, D. Murdock, M. G. D. Nix, T. A. A. Oliver and A. G. Sage, *Phys. Chem. Chem. Phys.*, 2010, **12**, 1218–1238.
34 L. H. Andersen, G. Aravind, R. Antoine, B. Klaerke, J. Lemoine, A. Racaud, D. B. Rahbek, J. Rajput and P. Dugourd, *Phys. Chem. Chem. Phys.*, 2010, **12**, 3486–3490.
35 B. Cronin, M. G. D. Nix, R. H. Qadiri and M. N. R. Ashfold, *Phys. Chem. Chem. Phys.*, 2004, **6**, 5031–5041.

36 A. Iqbal, M. S. Y. Cheung, M. G. D. Nix and V. G. Stavros, *J. Phys. Chem. A*, 2009, **113**, 8157–8163.
37 K. Siriwong, A. A. Voityuk, M. D. Newton and N. Rosch, *J. Phys. Chem. B*, 2003, **107**, 2595–2601.
38 P. Ball, *Chem. Rev.*, 2008, **108**, 74–108.
39 A. R. McKay, M. E. Sanz, C. R. S. Mooney, R. S. Minns, E. M. Gill and H. H. Fielding, *Rev. Sci. Instrum.*, 2010, **81**, 123101.
40 J. P. Kehrer, *Crit. Rev. Toxicol.*, 1993, **23**, 21–48.
41 B. J. Whitaker, ed., *Imaging in Molecular Dynamics: Technology and Applications*, Cambridge University Press, Cambridge, UK, 2003.
42 K. L. Wells, G. Perriam and V. G. Stavros, *J. Chem. Phys.*, 2009, **130**, 074304.
43 U. Even, J. Jortner, D. Noy, N. Lavie and C. Cossart-Magos, *J. Chem. Phys.*, 2000, **112**, 8068–8071.
44 G. M. Roberts, J. L. Nixon, J. Lecointre, E. Wrede and J. R. R. Verlet, *Rev. Sci. Instrum.*, 2009, **80**, 053104.
45 C. A. Williams, G. M. Roberts, H. Yu, N. L. Evans, S. Ullrich and V. G. Stavros, *J. Phys. Chem. A*, 2011, DOI: 10.1021/jp2053212.
46 A. L. Devine, B. Cronin, M. G. D. Nix and M. N. R. Ashfold, *J. Chem. Phys.*, 2006, **125**, 184302.
47 I. C. Walker, M. H. Palmer, M. J. Hubin-Franskin and J. Delwiche, *Chem. Phys. Lett.*, 2003, **367**, 517–522.
48 D. J. Hadden, K. L. Wells, G. M. Roberts, L. T. Bergendahl, M. J. Paterson and V. G. Stavros, *Phys. Chem. Chem. Phys.*, 2011, **13**, 10342–10349.
49 M. Barbatti, H. Lischka, S. Salzmann and C. M. Marian, *J. Chem. Phys.*, 2009, **130**, 034305.
50 K. A. Holbrook, M. J. Pilling and S. H. Robertson, *Unimolecular Reactions*, John Wiley and sons, Chicester, UK, 1996.
51 R. Crespo-Otero, M. Barbatti, H. Yu, N. L. Evans and S. Ullrich, *ChemPhysChem*, 2011, **12**, 3365–3375.
52 G. da Silva, E. E. Moore and J. W. Bozzelli, *J. Phys. Chem. A*, 2006, **110**, 13979–13988.
53 G. da Silva, *Chem. Phys. Lett.*, 2009, **474**, 13–17.
54 D. A. Blank, S. W. North and Y. T. Lee, *Chem. Phys.*, 1994, **187**, 35–47.
55 M. Barbatti, M. Vazdar, A. J. A. Aquino, M. Eckert-Maksic and H. Lischka, *J. Chem. Phys.*, 2006, **125**, 164323.
56 G. A. King, T. A. A. Oliver and M. N. R. Ashfold, *J. Chem. Phys.*, 2010, **132**, 214307.
57 E. Nir, K. Kleinermanns and M. S. de Vries, *Nature*, 2000, **408**, 949–951.
58 M. Smits, C. A. de Lange, S. Ullrich, T. Schultz, M. Schmitt, J. G. Underwood, J. P. Shaffer, D. M. Rayner and A. Stolow, *Rev. Sci. Instrum.*, 2003, **74**, 4812–4817.
59 J. B. Fenn, *Angew. Chem., Int. Ed.*, 2003, **42**, 3871–3894.
60 J. Lecointre, G. M. Roberts, D. A. Horke and J. R. R. Verlet, *J. Phys. Chem. A*, 2010, **114**, 11216–11224.
61 A. Iqbal and V. G. Stavros, *J. Phys. Chem. Lett.*, 2010, **1**, 2274–2278.
62 F. F. Crim, *Nat. Chem.*, 2011, **3**, 344–345.